RSC Advances

PAPER

View Article Online
View Journal | View Issue

Cite this: *RSC Adv.*, 2020, **10**, 17524

Polypyrrole modified magnetic reduced graphene oxide composites: synthesis, characterization and application for selective lead adsorption†

Zhanmeng Liu, *[ab] Zhimin Gao,[a] Lichun Xu[a] and Fengping Hu[a]

To enhance the ability to remove lead from water, polypyrrole modified magnetic Fe_3O_4/reduced graphene oxide composites (PPy-FG) were prepared *via in situ* polymerization and employed for the Pb(II) adsorption. The physicochemical structure and adsorption mechanism of the prepared magnetic PPy-FG were studied *via* vibrating sample magnetometer, X-ray diffraction, scanning electron microscopy, Fourier transform infrared spectroscopy, Brunauer–Emmett–Teller analysis, and X-ray photoelectron spectroscopy. The effects of several factors on Pb(II) adsorption were evaluated, including pH value, temperature, and competitive ions. Under the optimal conditions (pH 5 and 298 K), the maximum adsorption capacity of PPy-FG was 93.2 mg g^{-1} giving an improvement of 31% over that of 71 mg g^{-1} for Fe_3O_4/reduced graphene oxide (Fe_3O_4/rGO). Moreover, the experimental data were well fitted with the Langmuir adsorption model and the pseudo-second-order kinetics model, indicating that the adsorption process was mainly a monolayer chemical adsorption. Thermodynamic studies revealed a spontaneous and endothermic adsorption process. The selective adsorption of Pb(II) by PPy-FG is superior to that of Fe_3O_4/rGO in the presence of similar metals in the same medium. In addition, the adsorption performance of PPy-FG showed great potential in the remediation of heavy metal contaminated water through using its magnetic properties and excellent affinity for heavy metals.

Received 18th February 2020
Accepted 23rd April 2020

DOI: 10.1039/d0ra01546f

rsc.li/rsc-advances

1. Introduction

In recent years, with the continuous development of the global industry and economy, a large amount of industrial wastewater containing heavy metals has been directly discharged into natural water bodies without any treatment, such that the content of heavy metals in water environments has risen sharply.[1–3] Because heavy metals are difficult to degrade in nature and have long-lasting toxicity and bioaccumulation, they pose a serious threat to the stability of the ecological environment and human production and life.[4] Lead (Pb) is a common non-biodegradable heavy metal that can cause kidney damage, anemia, hemolysis, liver dysfunction and nerve cell damage.[5,6] Lead content is clearly defined in the World Health Organization (WHO) has set an maximum allowable level of lead in drinking water to 0.01 mg L^{-1}.[7] Therefore, it is necessary to develop a method for effectively removing lead in water as soon as possible.

To date, many method have been applied to the removal of Pb(II) from water, including precipitation method, electrolysis method, ion exchange method, membrane separation method, and adsorption method.[8,9] However, most of these methods are expensive to operate and may even cause other contamination. Compared with other methods, adsorption method has the advantages simple operation, cost-effectiveness, and environmental friendliness,[10,11] so it is commonly used to treat wastewater containing heavy metal ions.[12] The removal efficiency of adsorption method on pollutants from water mainly depends on the self-properties of sorbent, and the development of novel sorbent has always been one of hotpots in the field of wastewater treatment.

Graphene is widely used in many industries due to its excellent physicochemical properties.[13,14] Graphene oxide (GO) has a large surface area and a large number of functional groups such as hydroxyl groups, carboxyl groups, and epoxy groups, which provide abundant active adsorption sites for various contaminants and functionalized attachment sites in aqueous solutions.[15] In addition, GO is more environmentally friendly and has better biocompatibility than other carbonaceous nanomaterials.[16] Therefore, it is considered an ideal sorbent for water purification. For example, poly(amidoamine) modified graphene oxide *via* a grafting-from method, and could be applied to removal of heavy metal ions.[17]

[a]*School of Civil Engineering and Architecture, East China Jiao Tong University, Nanchang, 330013, China. E-mail: ustblzm@sina.com; gzm5683@sina.com; 1770660095@qq.com; 2452402815@qq.com*

[b]*School of Civil Engineering and Architecture, Nanchang Institute of Technology, Nanchang 330099, China*

† Electronic supplementary information (ESI) available. See DOI: 10.1039/d0ra01546f

However, graphene and GO are easy to agglomerate in water and difficult to separate,[18] which limited their widely application in environmental pollutant management. Therefore, magnetic graphene-based sorbents have become a research hotspot due to their easy separation characteristics. For example, Cao *et al.*[19] fabricated Fe_3O_4/rGO hybrid nanocomposites was used to Pb(II) removal and the maximum adsorption capacity was 30.68 mg g^{-1}. Sun *et al.*[20] reported a magnetic graphene nanocomposites modified with ionic liquids for Pb(II) removal and the maximum adsorption capacity was 85 mg g^{-1}. However, there exist two obvious defects: (i) these sorbents show a low adsorption capacity for Pb(II); (ii) iron nanoparticles are susceptible to oxidation in acidic solution.[21] For the purpose of overcome this problem, some shell structure or decorative materials are usually introduced, including a silica, metal shell, and polymer.[21,22]

Polypyrrole (PPy) is one of most intensively researched polymers due to its simple synthesis, high conductivity, good biocompatibility, unique electronic, and redox properties.[23] The positively charged nitrogen atoms in PPy may presents a great affinity toward to heavy metal.[24] For instance, the PPy/multi-walled carbon nanotube composite can be used as an efficient sorbent for removal of Pb(II) from aqueous solutions.[25] Karthik, R *et al.*[26] demonstrated that using chemically modified chitin with PPy as an sorbent for the removal of Pb(II) ions from aqueous solution had a great potential application. However, using magnetic graphene-based materials with PPy for Pb(II) removal from water has not been reported so far.

In this study, the magnetic PPy-FG composites were synthesized *via in situ* polymerization and the objective of this paper focused on enhancing the removal of Pb(II) by decorating Fe_3O_4/rGO composites with PPy. The samples were characterized *via* X-ray diffraction (XRD), vibrating sample magnetometer (VSM), scanning electron microscopy (SEM), Fourier transform infrared spectroscopy (FTIR), Brunauer–Emmett–Teller (BET), zeta potential, and X-ray photoelectron spectroscopy (XPS) to study its micro-structural morphology and adsorption mechanism. Furthermore, the effects of parameters on Pb(II) adsorption were investigated, including pH value, competitive ions, and temperature.

2. Materials and experiments

2.1. Materials

Graphite powder, H_2O_2 (30%), H_2SO_4, CH_3COONa, HCl (37%), HNO_3 (65%), polyvinylpyrrolidone (PVP), absolute ethyl alcohol (CH_3CH_2OH), ethylene glycol ($(CH_2OH)_2$), $FeCl_3 \cdot 6H_2O$, $KMnO_4$, $NaNO_3$, and NaOH were purchased from Xilong Chemical Engineering Company, Ltd., China. Pb $(NO_3)_2$, and ammonium persulfate was obtained from the Beijing Chemical Factory, China. Pyrrole monomer was obtained from Aldrich. All chemical reagents were of analytical grade and were used as received. The distilled water was used throughout the experiments. GO was prepared from graphite powder using the modified Hummers' method.[27]

2.2. Preparation of Fe_3O_4/rGO

0.3 g of the GO was ultrasonically uniformly dispersed in 30 mL of $(CH_2OH)_2$ for 2 h. Then, 1.32 g of CH_3COONa and 1.25 g of $FeCl_3 \cdot 6H_2O$ were added to the above solution and stirred for 30 min, and the mixed solution was transferred to a polytetrafluoroethylene reactor and reacted at 200 °C for 10 h. In the end, a black precipitate was obtained by centrifugation, which was washed three times with ethanol and distilled water, respectively, and then vacuum dried at 60 °C for 24 h to obtain a product which was Fe_3O_4/rGO.

2.3. Synthesis of PPy-FG

The PPy-FG composite general synthesis process can be briefly described as follows: firstly, 0.5 g of the magnetic Fe_3O_4/rGO was added into 100 mL PVP (2 g L^{-1}) solution, and ultrasonically dispersed for 2 h. Next, 1 mL pyrrole monomer and $FeCl_3 \cdot 6H_2O$ (1.5 g) was dissolved into above mixed solution and stirred for 5 h at room temperature. Finally, the obtained products were washed three times with ethanol and distilled water, respectively, and dried at 60 °C for 12 h in a vacuum oven. The product obtained was labeled as PPy-FG.

2.4. Characterization and apparatus

The magnetic properties of the prepared materials were measured through VSM (model PPMS-9T, USA). To determine the crystalline phases in the solid sorbent, the materials were analyzed by XRD using a D/max-2500/pc diffractometer with Cu-Kα radiation. The surface morphology of the sorbent was examined by SEM (model Hitachi SU-8010, Japan). FTIR spectra were obtained by a Nicolet 6700 spectrophotometer. In addition, the surface area and the pore size distribution of the sorbent were measured by N_2 adsorption–desorption test (Autosorb-iQ2, Quantachrome Instruments, USA) at 77 K over a relative pressure ranging from 0 to 1.0. XPS (PHI-5000 Versaprobe I) was performed to analyze the chemical element composition of sorbent. The zeta (ζ) potential was measured using Malvern ZEN 3600 Dynamic Light Scattering (DLS), and pH was measured using a pH Meter (model SJ-3F).

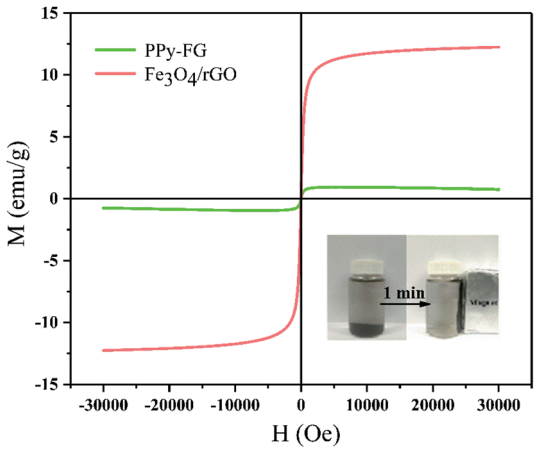

Fig. 1 Hysteresis loops of magnetic Fe_3O_4/rGO and PPy-FG.

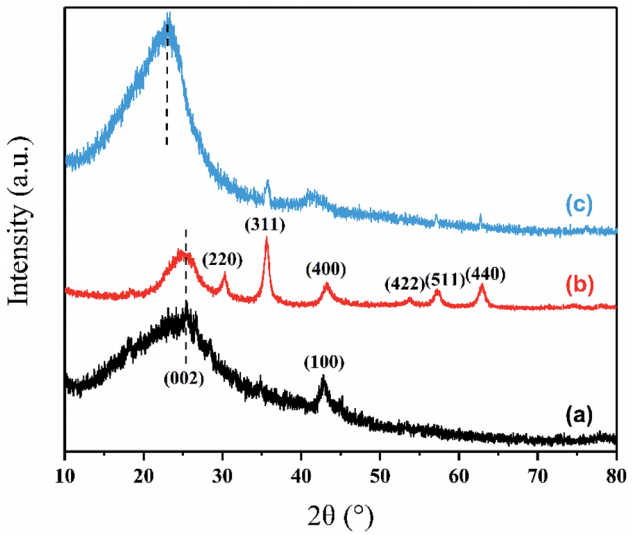

Fig. 2 XRD patterns of (a) rGO, (b) Fe_3O_4/rGO and (c) PPy-FG.

2.5. Lead adsorption experiments

Batch experiments were designed to study the effects of various factors and to explore adsorption kinetics, isotherms and thermodynamics parameters. Synthetic wastewater containing Pb(II) ion (30 mg L^{-1}) was extracted in the amount of 50 mL into 200 mL conical flasks and the pH value of the solution was adjusted using 0.1 M HCl or 0.1 M NaOH solution. With a certain amount of sorbent added, the conical flasks were shaken with a digital speed thermostat shaker at 200 rpm for 3 h to reach equilibrium. The adsorption kinetics for Pb(II) were studied with the initial concentration of 30 mg L^{-1} at room temperature (298 K). The adsorption isotherms for Pb(II) were established by initial concentrations ranging from 10 to 150 mg L^{-1} at 298 K. The adsorption thermodynamic for Pb(II) was investigated with the initial concentration of 30 mg L^{-1} at different temperature (283–313 K). The collected saturated sorbents were mixed with 20 mL of 0.2 M HNO_3 solution and shaken for 2 h for full desorption. Pb(II) concentrations in all experiments were achieved by AAS (model AA280FS, Agilent). Each test was conducted in triplicated, and the results reported in this paper were the arithmetic average of the three tests.

The adsorption capacity and removal efficiency of Pb(II) adsorbed on sorbents was calculated by the following equation (eqn (1) and (2)):

$$R\ (\%) = \frac{(C_0 - C_e)}{C_0} \times 100\% \quad (1)$$

$$q_e = \frac{(C_0 - C_e) \times V}{m} \quad (2)$$

where R (%) represents the removal efficiency and C_0 (mg L^{-1}) is the initial concentration of Pb(II). C_e (mg L^{-1}) represents the adsorption equilibrium concentration of Pb(II), q_e (mg g^{-1}) is the adsorption capacity of the sorbent, m (g) is the weight of the sorbent and V (L) is the volume of the solution.

2.6. Selectivity experiments

The competitive adsorption experiments, in order to investigate the selectivity of PPy-FG and Fe_3O_4/rGO, were conducted by preparing mixture containing Pb^{2+} and other ions (Zn^{2+}, Cd^{2+}, Ni^{2+}, Hg^{2+}) at pH 5.0. The initial concentration of each metal ion was 30.0 mg L^{-1} and the dosage of sorbent was 0.4 g L^{-1}. The concentration of each ion in the remaining solution was measured by ICP-AES after adsorption equilibrium. Distribution coefficients (K_d), selectivity coefficient (K) and relative selectivity coefficient (K_0) were obtained according to the following formula (eqn (3)–(5)):

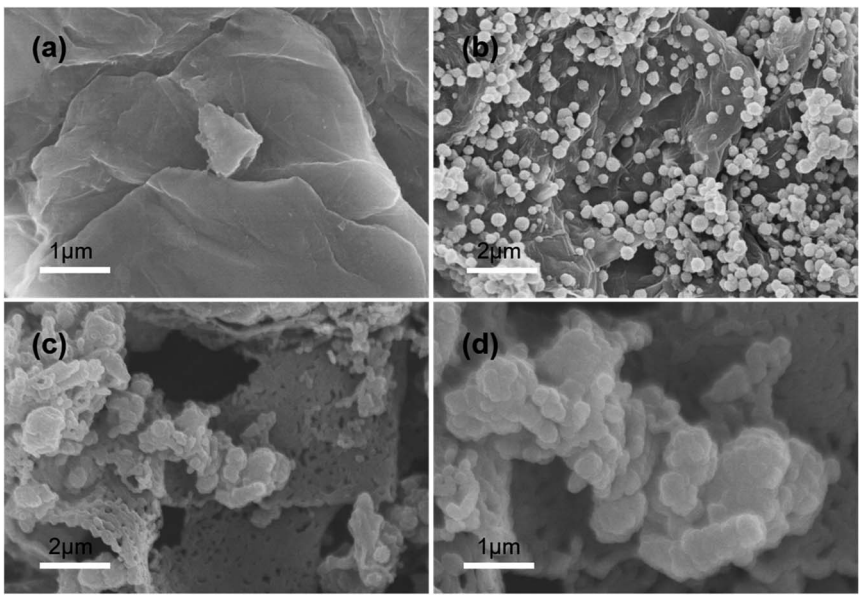

Fig. 3 SEM images of (a) GO, (b) Fe_3O_4/rGO, and (c and d) PPy-FG.

$$K_d = \frac{(C_0 - C_e)}{C_0} \times \frac{V}{m} \quad (3)$$

$$K = \frac{K_d(Pb^{2+})}{K_d(M^{2+})} \quad (4)$$

$$K_0 = \frac{K_a}{K_b} \quad (5)$$

where K_d represents the distribution coefficient (L g^{-1}). C_0 (mg L^{-1}) and C_e (mg L^{-1}) are initial and equilibrium concentration of metal ion, respectively. m (g) and V (L) are the dosage of sorbent and the volume of the solution, respectively. K is the selectivity coefficient of competitor metal ion M^{2+} with respects to Pb^{2+}. The larger K indicates a stronger choice ability for the Pb^{2+}. The larger of K_0 could indicate the enhanced extent of adsorption affinity and selectivity of PPy-FG (a) with respect to Fe_3O_4/rGO (b).

3. Results and discussion

3.1. Characterization of Fe_3O_4/rGO and PPy-FG

3.1.1. VSM analysis. Fig. 1 shows the magnetization hysteresis loops of the Fe_3O_4/rGO and PPy-FG. Saturation magnetization value of the Fe_3O_4/rGO and PPy-FG are 12.25 and 0.97 emu/g, respectively. The decline in the saturation magnetization value of PPy-FG may be attributed to the part magnetization of magnetic Fe_3O_4 nanoparticles was shielded by the electro-conductive PPy.[24] A test of the magnetic separation was conducted and was shown in Fig. 1(insert), the PPy-FG composite dispersed in aqueous solution can be achieved solid–liquid separation in approximately 1 min from water using a magnet after the Pb(II) decontamination. This indicated that the PPy-FG still had the property of magnetism after being used.

3.1.2. XRD analysis. The XRD patterns of as-prepared rGO, Fe_3O_4/rGO and PPy-FG are compared in Fig. 2. The wide diffraction peaks of the rGO appeared at $2\theta = 25.0°$ and 44.0°, correspond to the diffraction patterns of the crystallographic planes (002) and (100) of the graphene material.[28] Furthermore, the magnetic Fe_3O_4/rGO had a diffraction peak of Fe_3O_4 at $2\theta =$ 30.1°, 35.6°, 43.1°, 53.4°, 57.0° and 62.5°. These peaks correspond to the (220), (311), (400), (422), (511) and (440) crystal plane diffraction peaks, respectively(Joint Committee on Powder Diffraction System, JCPDS 75-0449).[19] This indicated that Fe_3O_4 load was successful and the magnetic Fe_3O_4/rGO was successfully prepared. In addition, there are weakened diffracted signal for the rGO sheets in Fe_3O_4/rGO in comparison with the pure rGO, which may be ascribed to that the strong signals of Fe_3O_4 cover the weak carbon peaks.[24] The characteristics rGO peak in Fe_3O_4/rGO shift from $2\theta = 25.0°$ to $2\theta =$ 23.02° after the addition of PPy (Fig. 2(c)), indicating the PPy was inserted between the rGO layers. Moreover, almost similar XRD patterns of PPy-FG with that of Fe_3O_4/rGO and rGO is observed. It is indicated that the PPy-FG composite has been successfully prepared.

3.1.3. SEM analysis. The surface morphology of GO, Fe_3O_4/rGO and PPy-FG were characterized using SEM. Fig. 3(a) shows that the prepared graphene oxide had a sheet-like structure with some wrinkles, indicating that the prepared graphene oxide had a relatively high degree of oxidation and the number of layers of graphene oxide is relatively large. The graphene oxide sheets were stacked together due to covalent bond polymerization between graphene oxide sheets.[29] Fig. 3(b) presents microstructural images of the Fe_3O_4/rGO. It can be seen from the figure that a mass of particles closely attaches on the surface of rGO sheets after the addition of Fe^{3+}, indicating the formation of loosely packed Fe_3O_4 nanoparticles onto rGO sheets. Furthermore, the phenomenon of aggregation–accumulation on the surface of graphene was weakened due to the presence of Fe_3O_4 nanoparticles. After dispersing the Fe_3O_4/rGO in the presence of PVP, the pyrrole monomers could be quickly forming a network structure and interweaves with Fe_3O_4/rGO by electrostatic attraction (Fig. 3(c and d)). The network structure of PPy, which makes the magnetic PPy-FG surface have more heavy metal adsorption sites, so it has better adsorption property.

3.1.4. FTIR analysis. The FTIR spectra of GO, Fe_3O_4/rGO, and PPy-FG were shown in Fig. 4. In the spectrum of Fe_3O_4/rGO and PPy-FG, the characteristic absorption peaks at 3410–3440, 1560–1630, 1473.35, and 1100–1200 cm^{-1} could be correspond to O–H, C=C, pyrrole ring, and C–O stretching, respectively. Moreover, the characteristic peaks at 510.82 and 513.98 cm^{-1} can be attribute to Fe–O stretching vibrations of iron oxide.[30] All these results demonstrate that the Fe_3O_4/rGO and PPy-FG has been synthesized successfully.

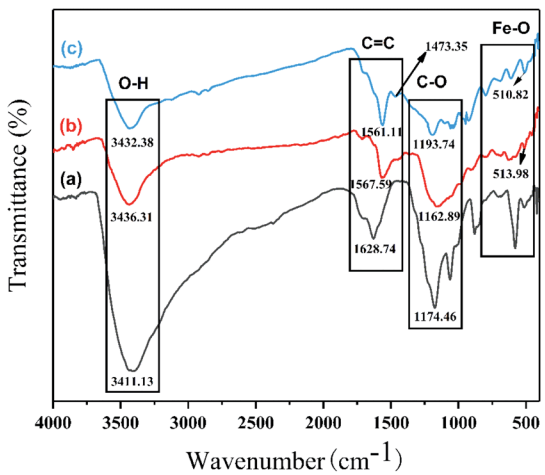

Fig. 4 FTIR spectra of (a) GO, (b) Fe_3O_4/rGO, and (c) PPy-FG.

Table 1 The results of BET analysis

Sorbent	BET surface area (m^2 g^{-1})	Total pore volume (cm^3 g^{-1})	Average pore diameter (nm)
Fe_3O_4/rGO	68	0.149	22
PPy-FG	33	0.204	28

3.1.5. BET analysis. BET analysis showed that the specific surface area was notably decreased from 68 $m^2\ g^{-1}$ for Fe_3O_4/rGO to 33 $m^2\ g^{-1}$ for PPy-FG (Table 1). There may be two reasons for the reduction in surface area after addition of PPy: (i) the large and continuous chain-like PPy on the Fe_3O_4/rGO surface blocking the porous network of Fe_3O_4/rGO composite;[24]; (ii) the chain-like PPy area might be close to zero and the decrease could be related to the mass contribution of PPy. The total pore volume and average pore diameter of the prepared magnetic PPy-FG were 0.204 $cm^3\ g^{-1}$ and 28 nm, respectively. Fig. S1† shows the nitrogen adsorption–desorption isotherms and pore size distribution curves of Fe_3O_4/rGO (a) and PPy-FG (b). From Fig. S1,† the adsorption capacity of the sorbent in the low-pressure section increases slowly with the increase of P/P_0, and the nitrogen molecule in the interval is adsorbed on the inner surface of the pores of as-prepared materials in the form of single layer. Moreover, the as-prepared materials increase sharply in the P/P_0 = 0.4/0.8–1.0 range, there is an obvious desorption hysteresis loop on the nitrogen desorption curve. The reason for these changes is capillary condensation of nitrogen in the pores of the as-prepared materials. According to the IUPAC (International Union of Pure and Applied Chemistry) classification, the nitrogen adsorption–desorption isotherms for the Fe_3O_4/rGO and PPy-FG composites all show type IV curve and H_3 hysteresis loop.[31] The change of the adsorption capacity of the magnetic Fe_3O_4/rGO and PPy-FG in the interval indicated that they were mesoporous material. These mesopores can greatly increase the specific surface area of the sorbents and make it have better adsorption performance.

3.2. Effect of pH

The pH was a critical factor in the process of heavy metal ions adsorption.[32] The effect of pH value on Pb(II) adsorption was determined over an initial pH ranged from 2 to 6, due to the form of lead ions is gradually converted from Pb(II) to Pb $(OH)_2$ precipitation when the pH value was greater than 6.[33] The Pb(II) adsorption performance and zeta potential of Fe_3O_4/rGO and PPy-FG are shown in Fig. 5. It can be seen that the Pb(II) adsorption performance of Fe_3O_4/rGO and PPy-FG exhibited similar increased trends along with the increasing pH value. This may be due to reduce the competitive adsorption of H^+ and Pb^{2+} in solution as the increase pH increased. Moreover, as the

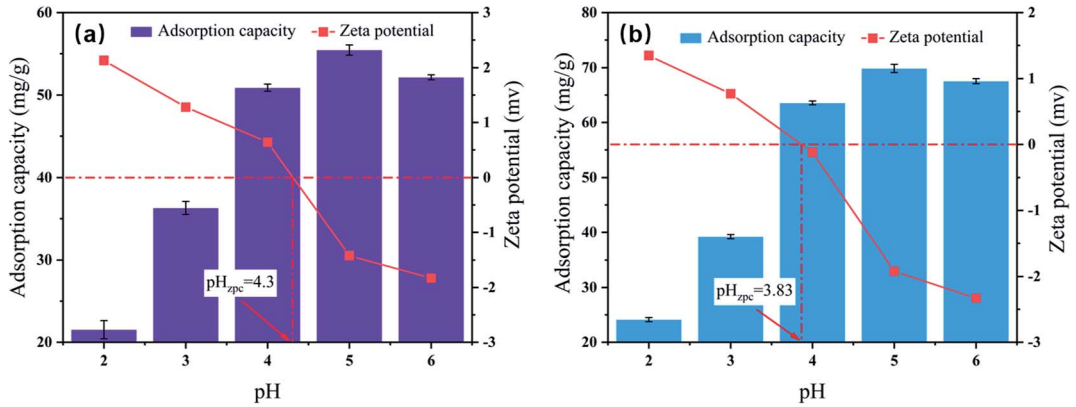

Fig. 5 Effect of initial pH on Pb(II) adsorption and zeta potential of Fe_3O_4/rGO (a) and PPy-FG (b) (pH 2–6, Pb(II) ion concentration 30 mg L^{-1}, sorbent dosage 0.4 g L^{-1}, time 3 h, T 298 K).

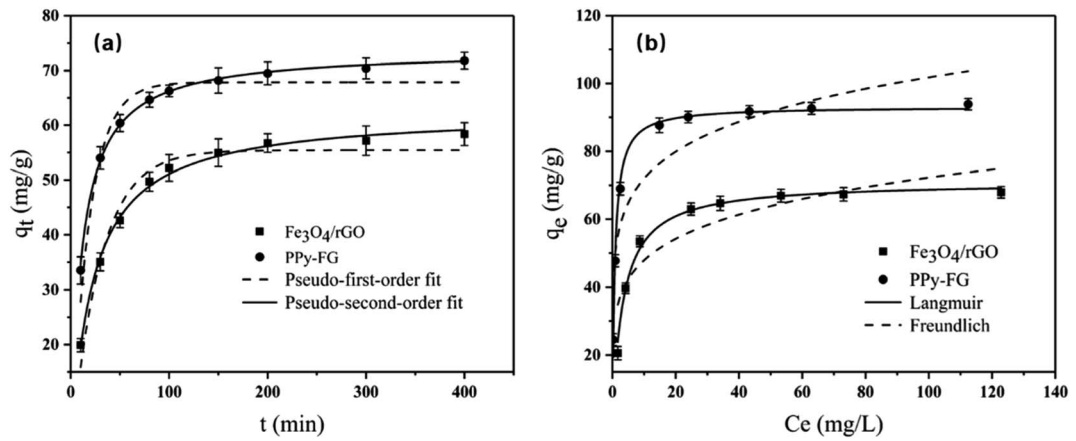

Fig. 6 (a) Adsorption kinetics (pH 5, Pb(II) ion concentration 30 mg L^{-1}, sorbent dosage 0.4 g L^{-1}, T 298 K, time 10–400 min) and (b) adsorption isotherms (pH 5, time 3 h, sorbent dosage 0.4 g L^{-1}, T 298 K, initial Pb(II) concentration ranging from 10 to 150 mg L^{-1}) of Fe_3O_4/rGO and PPy-FG.

Table 2 The parameter of fitting curve for adsorption kinetics equation

	Pseudo-first-order kinetic equation			Pseudo-second-order kinetic equation		
Sorbent	q_e (mg g^{-1})	k_1/min^{-1}	R^2	q_e (mg g^{-1})	k_2/(g mg^{-1}·min^{-1})	R^2
Fe_3O_4/rGO	55.43	0.033	0.961	62.40	0.0007	0.997
PPy-FG	67.85	0.053	0.897	73.68	0.0012	0.998

Table 3 The parameter of fitting curve for adsorption isotherms equation

	Langmuir			Freundlich		
Sorbent	Q_m (mg g^{-1})	K_L (L mg^{-1})	R^2	K_F (mg$^{1-(1/n)}$ L$^{1/n}$ g^{-1})	n	R^2
Fe_3O_4/rGO	71.0	0.30	0.989	31.77	5.60	0.779
PPy-FG	93.2	1.30	0.990	50.87	6.63	0.847

pH value increases, some oxygen-containing functional groups on the sorbent was ionized can enhance the adsorption efficiency. According to the experimental results, the optimal pH value is 5, and the adsorption capacity reached to 55.3 mg g^{-1} and 69.9 mg g^{-1} for Fe_3O_4/rGO and PPy-FG, respectively. The species of Pb(II) may be presented in the form of Pb^{2+}, $Pb(OH)^+$, $Pb(OH)_2^0$ and $Pb(OH)_3^-$ at various pH values.[34] Thus, the species of $Pb(OH)_2^0$ are present at pH 6 leading to reduction in the adsorption capacity.[35]

The zero-potential charge of Fe_3O_4/rGO and PPy-FG are 4.30 and 3.83, respectively. The surface of sorbents was positively charged at pH range of 2 to 4, there was electrostatic repulsion between sorbents and Pb(II) in solution, which were unfavorable for the Pb(II) adsorption. At pH 5–6, the zeta potential of the sorbents surface was negative, indicating that the charge carried by the sorbents was negative. Hence, there was electrostatic attraction between sorbent and Pb(II) in the aqueous solution, which contributed to the adsorption of Pb(II).

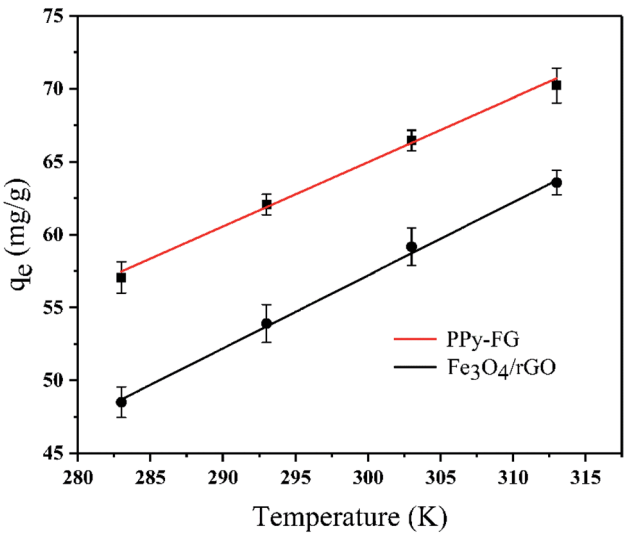

Fig. 7 Effect of temperature on Pb(II) adsorption (Pb(II) concentration 30 mg L^{-1}, sorbent dosage 0.4 g L^{-1}, time 3 h, pH 5, T 283–313 K).

3.3. Adsorption kinetics and isotherms

Adsorption kinetics tests of Pb(II) were determined to evaluate the different adsorption behavior of Fe_3O_4/rGO and PPy-FG. As shown in Fig. 6(a), the adsorption of Pb(II) ion proceeded rapidly during the initial 100 min and finally reached equilibrium in 3 h. The pseudo-first-order equation and pseudo-second-order equation are given Table. S1.†

The pseudo-first order and pseudo-second order were validated based on the correlation coefficient (R^2) and the kinetic parameters are listed in Table 2. In comparison to the pseudo-first order, the experiment data of Fe_3O_4/rGO and PPy-FG are well fitted to pseudo-second-order kinetics (R^2 > 0.997), indicating that the rate-determining step is the chemisorption rather than diffusion in present system.[36] PPy-FG composites produced by PPy decorated Fe_3O_4/rGO increased the adsorption capacity, suggesting that the PPy partially accounted for the enhanced Pb(II) adsorption.

Adsorption isotherms of Pb(II) on Fe_3O_4/rGO and PPy-FG were conducted under the initial concentration ranging from 10 to 150 mg L^{-1}. As displayed in Fig. 6(b), it was known that at room temperature condition, the adsorption capacity of Pb(II) by the Fe_3O_4/rGO and PPy-FG was gradually increasing with the increasing concentration of Pb(II) ions and finally got up to equilibrium. Two typical isotherm models (Langmuir and Freundlich) are used to fit the adsorption data. The equations and parameters description are given Table. S2.†

The isotherms parameters and the correlation coefficient (R^2) are shown in Table 3. Evidently, the experimental data was fitted better by the Langmuir model (R^2 > 0.989), suggesting that

Table 4 The parameter of fitting curve for adsorption thermodynamics equation

	ΔG^θ (kJ mol^{-1})				ΔH^θ (kJ	ΔS^θ (kJ
Sorbent	283 K	293 K	303 K	313 K	mol^{-1})	mol^{-1} K^{-1})
Fe_3O_4/rGO	−3.56	−4.65	−5.74	−6.83	27.29	0.109
PPy-FG	−4.63	−6.12	−7.61	−9.10	37.54	0.149

a mainly monolayer adsorption behavior on the prepared sorbents. The maximum adsorption capacity (Q_m) of PPy-FG (93.2 mg g^{-1}) was significantly higher than Fe_3O_4/rGO (71.0 mg g^{-1}). In addition, the Freundlich isotherm model fitting results ($1 < n < 10$) show that the sorbents is easy to absorb Pb(II) in aqueous solution under room temperature.[37]

3.4. Adsorption thermodynamics

The adsorption thermodynamic behavior can describe the energy change of magnetic Fe_3O_4/rGO and PPy-FG adsorption of Pb(II). The thermodynamic parameters, including the Gibb's free energy (ΔG^θ), enthalpy (ΔH^θ) and entropy (ΔS^θ) can be calculated *via* the Gibbs free energy and the Van't Hoff equation (Table S3†).[38] Form Fig. 7 and Table 4, the negative values of ΔG^θ indicated that the adsorption processes are spontaneous and feasible trend. ΔG^θ is more negative with higher temperature (283 K to 313 K), indicating that the temperature rising can increase the adsorption capacity of Fe_3O_4/rGO and PPy-FG. Moreover, the positive values of ΔH^θ confirmed the adsorption processes are endothermic, and the low positive values of ΔS^θ suggested that the randomness is moderately increased in the adsorption procedure.[39,40] Generally, the ΔH^θ with values between 20.9 and 418.4 kJ mol^{-1} is frequently considered as comparable values for the chemical adsorption processes.[41] The ΔH^θ value of Fe_3O_4/rGO and PPy-FG was found to be 27.29 and 37.54 kJ mol^{-1}, respectively. This result indicated that the transportation of Pb(II) from the aqueous solution to the sorbents surface occurred chemically.

3.5. Selectivity study

The selectivity of PPy-FG towards Pb(II) was investigated and results were presented in Fig. 8 and Table 5. The adsorption capacity onto PPy-FG towards Pb(II) was higher than other competitive ions, and the adsorption capacity of Pb(II) onto PPy-FG was higher than Fe_3O_4/rGO. Table 5 shows the K_d value of PPy-FG for Pb(II) was the largest, the relative selectivity coefficient K_0 of PPy-FG was high, indicating a higher selectivity for Pb(II) in the presence of similar metal in the same medium. In addition, competitive ions were also can applied to investigate competitive recognition.[37] Fig. 8 shows the equilibrium adsorption capacity of Pb(II) onto PPy-FG was 60.9 mg g^{-1}, which was quite higher than the adsorption capacity of other four analogues with 8.4, 30.2, 12.1 and 6.8 mg g^{-1}, respectively. The competitor encountered different abilities of recognition by PPy-FG though like Pb(II) in structure and charge, which could be demonstrated that PPy-FG also exhibited outstanding discrimination for Pb(II) in complicated samples. Therefore, the higher discrimination and selectivity of PPy-FG could benefit for Pb(II) removal.

Table 5 Competitive adsorption of different ions by PPy-FG and Fe_3O_4/rGO

	PPy-FG		Fe_3O_4/rGO		
Metal type	K_d (L g^{-1})	K_a	K_d (L g^{-1})	K_b	K_0
Pb(II)	10.798	—	3.813	—	—
Zn(II)	0.315	34.279	0.393	9.702	3.533
Cd(II)	1.690	6.389	1.078	3.537	1.806
Ni(II)	0.481	22.449	0.722	5.281	4.251
Hg(II)	0.249	43.365	0.194	19.654	2.206

3.6. Reusability study and comparison of PPy-FG with other sorbents

Reusability performance of sorbent is a significant factor for its practical application. 0.2 M HNO_3 solution was used for the regeneration in this study and the recovery removal rate of PPy-FG after desorption. From Fig. 9, the removal efficiency of Pb(II) decrease slightly with sequential cycles of reuse. Even after five desorption regenerations, the PPy-FG (85.7%) of removal efficiency on Pb(II), indicating that the magnetic PPy-FG composite has great potential as a reusable sorbent.

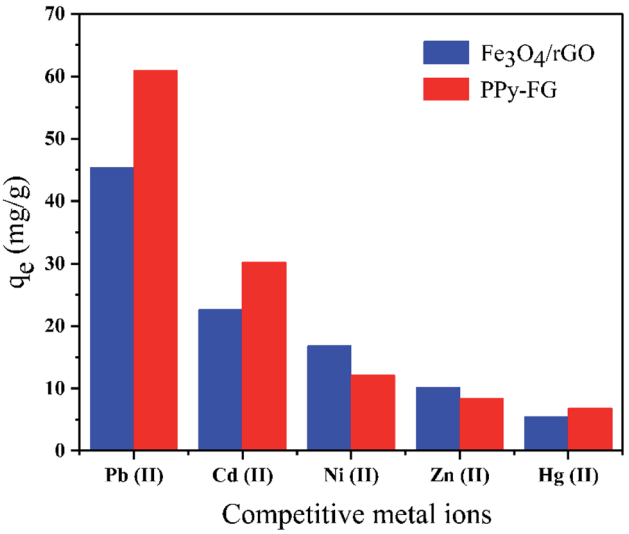

Fig. 8 Adsorption selectivity of Pb(II) onto PPy-FG and Fe_3O_4/rGO.

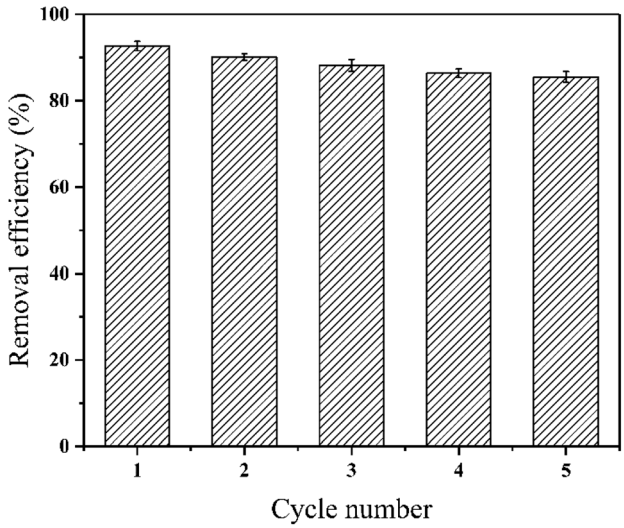

Fig. 9 Effect of cycling times on Pb(II) removal.

Table 6 Comparison of Q_m of different sorbents for Pb(II)

Sorbent	Q_m (mg g^{-1})	Conditions	Initial concentration (mg L^{-1})	References
Graphene nanosheets	35.5	pH 4.0, 30 °C	40	42
PPy-g-Ch	9.14	pH 6.0, 50 °C	10	26
PLAC	98.39	pH 5.0, 25 °C	60	43
Fe_3O_4/activated carbon	71.42	pH 6.0, 50 °C	50	44
MWCNTs/Fe_3O_4	41.77	pH 5.3, 30 °C	30	45
Fe_3O_4/rGO	71.0	pH 5.0, 25 °C	30	This work
PPy-FG	93.2	pH 5.0, 25 °C	30	This work

For comparison, the Q_m of different sorbents for the removal of Pb(II) as reported in literature[26,42–45] were shown in Table 6. The results indicated that PPy-FG prepared in this study is a promising sorbent for the Pb(II) adsorption than other sorbents. Furthermore, it can be easily separated from the aqueous solution based on the magnetism and achieved its reusability better. The great characteristics of PPy-FG bring us a potential method for selective Pb(II) adsorption from the water.

3.7. The mechanism of Pb(II) removal

To gain insight into the mechanism of Pb(II) removal, XPS analyses of PPy-FG composites were carried out before and after the adsorption of Pb(II). From Fig. 10(a), the presence of distinct Pb(II) binding energy peak in the full range XPS spectrum of PPy-FG after adsorption further confirmed the successful adsorption of Pb(II). From Fig. 10(b), the O 1s spectrum mainly has two peaks with binding energy of 533.25 eV and 531.83 eV, which could be corresponds to C–O, C–OH functional groups, respectively. It was found that the area ratio of C–O peak increased after Pb(II) adsorption, which was mainly attributed to the adsorbed H_2O. On the contrary, the relative contents of oxygen at the bonding energy of 531.83 eV decreased, indicating that the oxygen-containing groups on the rGO also contributed to the Pb(II) removal through chemisorption.[30] The Pb 4f spectrum (Fig. 10(c)) of PPy-FG after adsorption showed two peaks

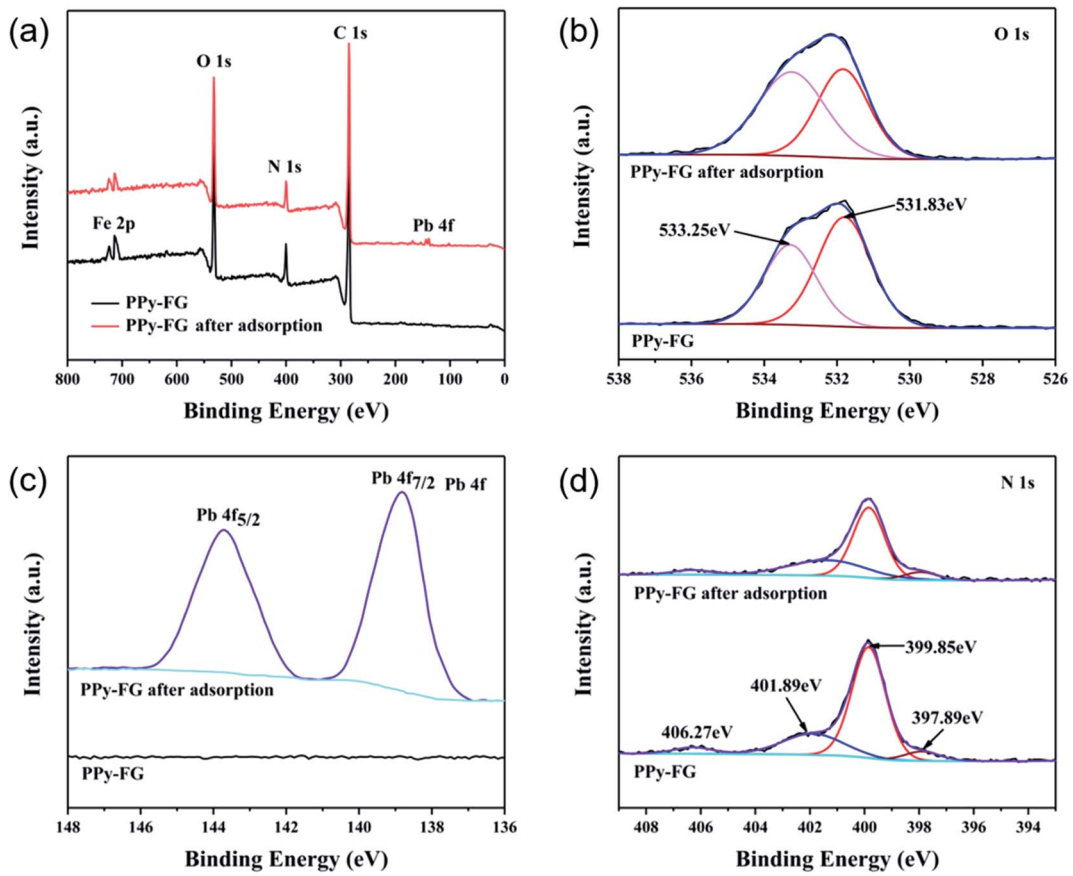

Fig. 10 XPS spectrum of survey (a), O 1s (b), Pb 4f (c), N 1s (d) of PPy-FG before and after Pb(II) adsorption.

Table 7 Leached percentage of iron in Fe_3O_4/rGO and PPy-FG under acidic medium

	Leached Fe content (%)							
	Fe_3O_4/rGO				PPy-FG			
HCl concentration	12 h	24 h	36 h	48 h	12 h	24 h	36 h	48 h
0.01 M	0.13	0.52	1.16	2.81	0.05	0.08	0.22	0.58
1.0 M	5.32	9.85	14.24	19.67	1.35	3.75	5.89	8.46

with the bonding energies of 143.7 and 138.8 eV, attributed to Pb $4f_{5/2}$ and Pb $4f_{7/2}$, respectively, indicating that the Pb bonded to O in the Pb(II) adsorption process.[46] The N 1s XPS spectrum of PPy-FG before and after adsorption is shown in Fig. 10(d). Four peaks at 406.27, 401.89, 399.85, and 397.89 eV, which could be originated from the π–π bond, positively charged nitrogen (N^+), benzenoid amine (–NH–), and quinoid imine (=N–), respectively. It was found that decrease under the binding energy of 399.85 eV, indicating that the nitrogen species of PPy also participated in the Pb(II) removal. In addition, the broad sheet structure of rGO and abundant surface area of Fe_3O_4 provide more sites to capture Pb(II).

3.8. Iron leaching studies

In order to evaluate the iron leaching rate of sorbents under acidic medium, 20 mg of Fe_3O_4/rGO and PPy-FG were separately suspended in solutions containing 50 mL (0.01, and 1.0 M) of HCl at different dispersion times (12, 24, 36, and 48 h). The leached amount of iron in the supernatant was measured by AAS (model AA280FS, Agilent). The leached percentage of iron in Fe_3O_4/rGO and PPy-FG under acidic medium are displayed in Table 7. It can be seen that the percentage of leaching of iron in both sorbents Fe_3O_4/rGO and PPy-FG in 0.01 M HCl for 12 h were 0.13% and 0.05%, respectively. For 12 h in 1.0 M HCl were 5.32% and 1.35%, respectively. Hence, the magnetic PPy-FG was more stability than Fe_3O_4/rGO.

4. Conclusions

The magnetic PPy-FG was successfully prepared *via in situ* polymerization, which a facile and low-cost process. The physicochemical structure and composition of Fe_3O_4/rGO and PPy-FG were well characterized. Compared to the Fe_3O_4/rGO, the PPy-FG showed desirable adsorption capacity toward Pb(II) ion and the maximum adsorption capacity for Pb(II) was up to 93.2 mg g^{-1} (298 K). The adsorption data were better matched with the Langmuir adsorption model and the pseudo-second-order kinetics model, indicating the dominant role of monolayer chemisorption. Furthermore, the thermodynamic studies revealed that a spontaneous and endothermic adsorption process. The selective adsorption of Pb(II) by PPy-FG is superior to Fe_3O_4/rGO in the presence of similar metals in the same medium. In addition, the PPy-FG maintained good adsorption performance after multiple adsorption–desorption cycles, the removal efficiency of Pb(II) reached 85.7%, indicating that the sorbent has reusable value. The iron leaching studies showed that the magnetic PPy-FG was more stability than Fe_3O_4/rGO. All these results demonstrate that the PPy-FG could be used as a stable, efficient and reusable sorbent in the remediation of metal pollutants from wastewater.

Conflicts of interest

There are no conflicts of interest to declare.

Acknowledgements

This work was supported by the National Natural Sciences Foundation of China (No. 51468016) and the Natural Sciences Foundation of Jiangxi Province (No. 20171BAB206047).

References

1 P.-S. Keng, S.-L. Lee, S.-T. Ha, Y.-T. Hung and S.-T. Ong, *Environ. Chem. Lett.*, 2013, **12**, 15–25.
2 F. Fu and Q. Wang, *J. Environ. Manage.*, 2011, **92**, 407–418.
3 S. M. Mousa, N. S. Ammar and H. A. Ibrahim, *J. Saudi Chem. Soc.*, 2016, **20**, 357–365.
4 O. Tavakoli, V. Goodarzi, M. R. Saeb, N. M. Mahmoodi and R. Borja, *J. Hazard. Mater.*, 2017, **334**, 256–266.
5 X. Li, Z. Wang, Q. Li, J. Ma and M. Zhu, *Chem. Eng. J.*, 2015, **273**, 630–637.
6 M. Rashid, F. Khan and Lutfullah, *J. Water. Process. Eng.*, 2014, **3**, 53–61.
7 S. M. Samuel, S. S. Shah, J. Bhattacharya, K. Subramaniam and N. D. P. Singh, *Int. J. Biol. Macromol.*, 2018, **115**, 1142–1150.
8 Y. Yurekli, *J. Hazard. Mater.*, 2016, **309**, 53–64.
9 Md. Shahinul Islam, W. S. Choi, B. Nam, C. Yoon and H.-J. Lee, *Chem. Eng. J.*, 2017, **307**, 208–219.
10 I. Ali, Z. A. Al-Othman and A. Alwarthan, *J. Mol. Liq.*, 2016, **219**, 858–864.
11 I. Ali, M. Asim and T. A. Khan, *Int. J. Environ. Sci. Technol.*, 2012, **10**, 377–384.
12 S. Hokkanen, A. Bhatnagar and M. Sillanpaa, *Water Res.*, 2016, **91**, 156–173.
13 N. Zhang, M. Q. Yang, S. Liu, Y. Sun and Y. J. Xu, *Chem. Rev.*, 2015, **115**, 10307–10377.
14 C. Han, Z. Nan and Y. J. Xu, *Nano Today*, 2016, **11**, 351–372.
15 S. Kim, C. M. Park, M. Jang, A. Son, N. Her, M. Yu, S. Snyder, D. H. Kim and Y. Yoon, *Chemosphere*, 2018, **212**, 1104–1124.
16 S. Wan, F. He, J. Wu, W. Wan, Y. Gu and B. Gao, *J. Hazard. Mater.*, 2016, **314**, 32–40.
17 Y. Yang, G. Zhang, L. Yang, G. Zhang, F. Zhang and X. Fan, *Polym. Chem.*, 2013, **4**, 2164–2167.
18 Y. Zhang, L. Yan, W. Xu, X. Guo, L. Cui, L. Gao, Q. Wei and B. Du, *J. Mol. Liq.*, 2014, **191**, 177–182.
19 C. Wei, Y. Ma, Z. Wei and G. Lin, *Chem. Res. Chin. Univ.*, 2015, **31**, 508–513.
20 W. Sun, L. Li, C. Luo and L. Fan, *Int. J. Biol. Macromol.*, 2016, **85**, 246–251.

21 I. Larraza, M. Lopez-Gonzalez, T. Corrales and G. Marcelo, *J. Colloid Interface Sci.*, 2012, **385**, 24–33.
22 N. Ahmad, H. Sereshti, M. Mousazadeh, H. R. Nodeh, M. A. Kamboh and S. Mohamad, *Mater. Chem. Phys.*, 2019, **226**, 73–81.
23 M. Bhaumik, A. Maity, V. V. Srinivasu and M. S. Onyango, *J. Hazard. Mater.*, 2011, **190**, 381–390.
24 H. Wang, X. Yuan, Y. Wu, X. Chen, L. Leng, H. Wang, H. Li and G. Zeng, *Chem. Eng. J.*, 2015, **262**, 597–606.
25 E. Sahmetlioglu, E. Yilmaz, E. Aktas and M. Soylak, *Talanta*, 2014, **119**, 447–451.
26 R. Karthik and S. Meenakshi, *Int. J. Biol. Macromol.*, 2015, **78**, 157–164.
27 W. S. Hummers and R. E. Offeman, *J. Am. Chem. Soc.*, 1958, **208**, 1334–1339.
28 X. Lv, X. Xue, G. Jiang, D. Wu, T. Sheng, H. Zhou and X. Xu, *J. Colloid Interface Sci.*, 2014, **417**, 51–59.
29 L. Wei, Y. Wu, J. Chen and Y. Yang, *Crystengcomm*, 2013, **16**, 609–615.
30 L. Kong, Z. Li, X. Huang, S. Huang, H. Sun, M. Liu and L. Li, *J. Mater. Chem. A*, 2017, **5**, 19333–19342.
31 L. Meng, Y. Chan, H. Wang, Y. Dai, X. Wang and J. Zou, *Environ. Sci. Pollut. Res.*, 2016, **23**, 5122–5133.
32 X. Huang and M. Pan, *J. Mol. Liq.*, 2016, **215**, 410–416.
33 P. Hadi, J. Barford and G. McKay, *Environ. Sci. Technol.*, 2013, **47**, 8248–8255.
34 S. Yang, J. Hu, C. Chen, D. Shao and X. Wang, *Environ. Sci. Technol.*, 2011, **45**, 3621–3627.
35 M. Alsuhybani, A. Alshahrani, M. Algamdi, A. A. Al-Kahtani and A. A. Alqadami, *J. Mol. Liq.*, 2020, **301**, 112393.
36 A. K. Bhattacharya, T. K. Naiya, S. N. Mandal and S. K. Das, *Chem. Eng. J.*, 2008, **137**, 529–541.
37 L. Yan, H. Xiao, M. Meng, Z. Liu, N. Liang, X. Meng and Q. Jian, *Chem. Eng. J.*, 2016, **302**, 609–618.
38 E. C. Lima, A. Hosseini-Bandegharaei, J. C. Moreno-Piraján and I. Anastopoulos, *J. Mol. Liq.*, 2019, **273**, 425–434.
39 Y. Ren, H. A. Abbood, F. B. He, H. Peng and K. X. Huang, *Chem. Eng. J.*, 2013, **226**, 300–311.
40 X. Y. Yu, T. Luo, Y. X. Zhang, Y. Jia, B. J. Zhu, X. C. Fu, J. H. Liu and X. J. Huang, *Acs. Appl. Mater. Inter.*, 2011, **3**, 2585–2593.
41 L. Bai, H. Hu, W. Fu, J. Wan, X. Cheng, L. Zhuge, L. Xiong and Q. Chen, *J. Hazard. Mater.*, 2011, **195**, 261–275.
42 Z.-H. Huang, X. Zheng, W. Lv, M. Wang, Q.-H. Yang and F. Kang, *Langmuir*, 2011, **27**, 7558–7562.
43 L. Wang, J. Zhang, R. Zhao, Y. Li, C. Li and C. Zhang, *Bioresource Technol*, 2010, **101**, 5808–5814.
44 B. Kakavandi, R. R. Kalantary, A. J. Jafari, S. Nasseri, A. Ameri, A. Esrafili and A. Azari, *Clean: Soil, Air, Water*, 2015, **43**, 1157–1166.
45 L. Ji, L. Zhou, X. Bai, Y. Shao, G. Zhao, Y. Qu, C. Wang and Y. Li, *J. Mater. Chem.*, 2012, **22**, 15853–15862.
46 G. Konstantatos, L. Levina, A. Fischer and E. H. Sargent, *Nano Lett.*, 2008, **8**, 1446–1450.